Photocatalytic Degradation of Malachite Green and Rhodamine B Dye over SnO_2-CuO Binary Metal Oxide Nanocomposite under UV Light

A Dissertation
Submitted in partial fulfillment

FOR THE DEGREE
OF
MASTER OF SCIENCE IN CHEMISTRY

Under The Academic Autonomy
NATIONAL INSTITUTE OF TECHNOLOGY, ROURKELA

By
Jyoshna Marpally
410CY5062
Under the Guidance of
Dr. Priyabrat Dash

DEPARTMENT OF CHEMISTRY
NATIONAL INSTITUTE OF TECHNOLOGY
ROURKELA – 769008
ODISHA

May, 2015

CERTIFICATE

Dr.Priyabrat Dash
Assistant Professor
Department of Chemistry
NIT, Rourkela-ODISHA

This is to certify that the dissertation entitled ***"Photocatalytic degradation of malachite green and rhodamine B dye over CuO-SnO_2 binary metal oxide nanocomposite under UV light"*** *being submitted by* ***Jyoshna Marpally*** *to the Department of Chemistry, National Institute of Technology, Rourkela, Odisha, for the award of the degree of Master of Science in Chemistry is a record of bonafide research work carried out by her under my supervision and guidance. I am satisfied that the dissertation report has reached the standard fulfilling the requirements of the regulations relating to the nature of the degree*.

Rourkela-769008

Date:

Dr. Priyabrat Dash

(Supervisor)

ACKNOWLEDGEMENTS

First of all, I am thankful to my guide Dr. Priyabrat Dash who untiringly assisted me in my experiment and enhanced my knowledge base by making me aware about this experiment. My training would not have been successfully completed without the firm guidance of my guide who supervised me in my experiments.

I like to thank all faculty members of the Department of chemistry, who have always inspire me to work hard and helped me to learn new concepts and experiments during my stay at NIT, Rourkela.

I would like to thank my parents for their unconditional love and support. They have helped me in every situation throughout my life, I am grateful for their support.

I would like to accord my sincere gratitude to Mr. Aniket Kumar, Miss Lipeeka Rout and Miss Basanti Ekka for their valuable suggestions, guidance in carrying out experiments. Finally, I would like to thank all my lab mates Padmini, Anurag and Pradyuman for all fun times we had together in the lab.

Finally I would like to thank all my friends for their support and the great almighty to shower his blessing on us and making dreams and aspirations.

Jyoshna Marpally

Table of Contents

List of Figures

ABSTRACT

While the development of various metal and metal oxide based nanocomposites as photocatalyst materials is advancing over the years, the concurrent and rapid development of high surface active photocatalyst material such as binary metal oxide nanocomposite has provided remarkable promise in the development of a multifunctional photocatalysts. The p-n type binary metal oxide is the main centre of attraction. Traditionally available photocatalysts such as TiO_2, ZnO etc., lose their efficiency because of charge recombination. To overcome this problem, binary system such as SnO_2-CuO nanocomposite has been selected as it will synergistically hinder the charge recombination. Considering these benefits, we intend to synthesize a variety of novel SnO_2-CuO binary nanocomposite by sol-gel method. The nanocomposite will be characterized by FESEM, EDX, TGA, UV-Vis and Photoluminiscence measurements. The photocatalytic activities of SnO_2-CuO, evaluated using the photodegradation of malachite green and rhodamine B dyes under the irradiation of UV light, were also found to be related to the calcination temperature and the molar ratio of Cu to Sn. The maximum photocatalytic activity of the CuO-SnO_2 photocatalyst was observed to be calcined at 700°C for 2 h (the molar ratio of Cu to Sn was 1:1) due to the sample with good crystallization.

CHAPTER 1: INTRODUCTION

1.1: General Introduction

Environmental problems associated to hazardous wastes and toxic organic pollutants have been attracted a considerable attention due to its damage to human beings and aquatic animal. The development of new eco-friendly methods of destroying these pollutants became an imperative task.[1] Ultimately, research activities centered on advanced oxidation processes (AOPs) for the destruction of synthetic organic species resistant to conventional methods. Photocatalysis is one among those advanced oxidation processes (AOPs).[2] Photocatalysis rely on in situ generation of highly reactive radical species, mainly $HO\cdot$ by using solar, chemical or other forms of energy.[3] The most attractive feature of photocatalysis is that this highly potent and strongly oxidizing radical allows the destruction of a wide range of organic chemical substrate with no selectivity. Photocatalytic degradation of the organic pollutants from wastewater by semiconductor catalysts has pulled in extraordinary consideration throughout the years. Even though degradation begins with a partial degradation, the term 'photocatalytic degradation' usually refers to complete photocatalytic oxidation or photomineralization, essentially to CO_2, H_2O, NO_3^-, PO_4^{3-} and halide ions. [4]Organic pollutants include organic dyes which came up as one of the many new chemicals used in industrial activities. Due to the extensive use of these dyes in industries, they have become an integral part of industrial effluent. In fact, of the 450,000 ton of organic dyes annually produced worldwide, more than 11% is lost in effluents during manufacture and application processes. Most of these dyes are toxic and potentially carcinogenic in nature and their removal from the industrial effluents is a major environmental problem [5]. Various methods have been suggested to handle the dye removal from water; these include the biodegradation, coagulation, adsorption, advanced oxidation process(AOP) and the membrane process [6 7]. All these processes have some advantages or disadvantages over the other method. Among many dyes that are applied in manufacture products, malachite green (MG) and rhodamine-b (Rhb) must be highlighted. These dyes have an aromatic complex molecular structure defiant to degradation and can reduce the transmission of sunlight to water bodies, thereby affecting the aquatic biota of the habitat. Hence, MG and Rhb will produce irreversible damage to the environment if discharged into water. Among the photocatalysts, metal oxide semiconductors are the best choice

due to their distinctive properties, durability and cost effectiveness. Direct charge transfer between metal oxide and organic compounds is found as the dominant mechanism of photocatalysis. Reactive oxygen species, such as hydroxyl radicals also play a minor role in the photocatalysis. Many metal oxide such as ZnO,Nb_2O_3,SnO_2,Ni_2O_3,Al_2O_3,TiO_2 etc have been used for photocatalytic degradation of organic pollutants.[8] The photocatalyst titanium dioxide (TiO_2) is a wide band gap semiconductor(3.2 eV) and is successfully used as a photocatalyst for the treatment of organic [9] and dye pollutants[10]. Photocatalytic degradation of Reactive Orange 4 by various AOPs using UV and solar light has also been reported[11]. Among these metal oxides, semiconducting metal oxides proved to be efficient, whose valence band and conduction band are separated by an energy gap or band-gap. When a semiconductor molecule absorbs photons with energy equal or greater than its band-gap, electrons in the valence band can be excited and jump up into the conduction band, and thus charge carriers are generated. In order to have a photocatalysed reaction, the e^--h+ recombination, subsequent to the initial charge separation, must be prevented as much as possible.[12] SnO_2 and CuO are the most promising semiconducting metal oxide photocatalysts, as they possess a wide band gap, have high photosensitivity and low toxicity, besides their low cost. Introduction of bimetal oxides increases the band gap energy between valence band and conduction band and also enhances their photocatalytic activity, when compared to that of metal oxides.[13] Thus, research efforts have been made at exploiting new combination of photocatalysts. In this work we discussed SnO_2-CuO as the most efficient semiconductor photocatalyst for degradation of MG and Rhb.

1.2: Photocatalysis

Photocatalysis may be defined as a reaction which is accelerated in presence of a catalyst.[14] These reactions are initiated by absorption of a photon with sufficient energy (equal or higher than the band-gap energy (Ebg) of the catalyst).[15] [16] The absorption results in charge separation due to excited electron (e^-) from the valence band of the semiconductor catalyst to the conduction band, creating a hole (h+) in the valence.[17] The recombination of this electron and hole must be prevented for a favourable photocatalysed reaction.[18] Photocatalysis is widely being used in water and air purification,[19] self-cleaning surfaces,[20] self-sterilizing surfaces, photocatalytic lithography ,[21] microchemical systems,[22] selective and green synthesis of organic

compounds,[23] and the generation of hydrogen.[22f] There are many studies dealing with the photocatalytic decolorization of specific textile dyes from different chemical categories.

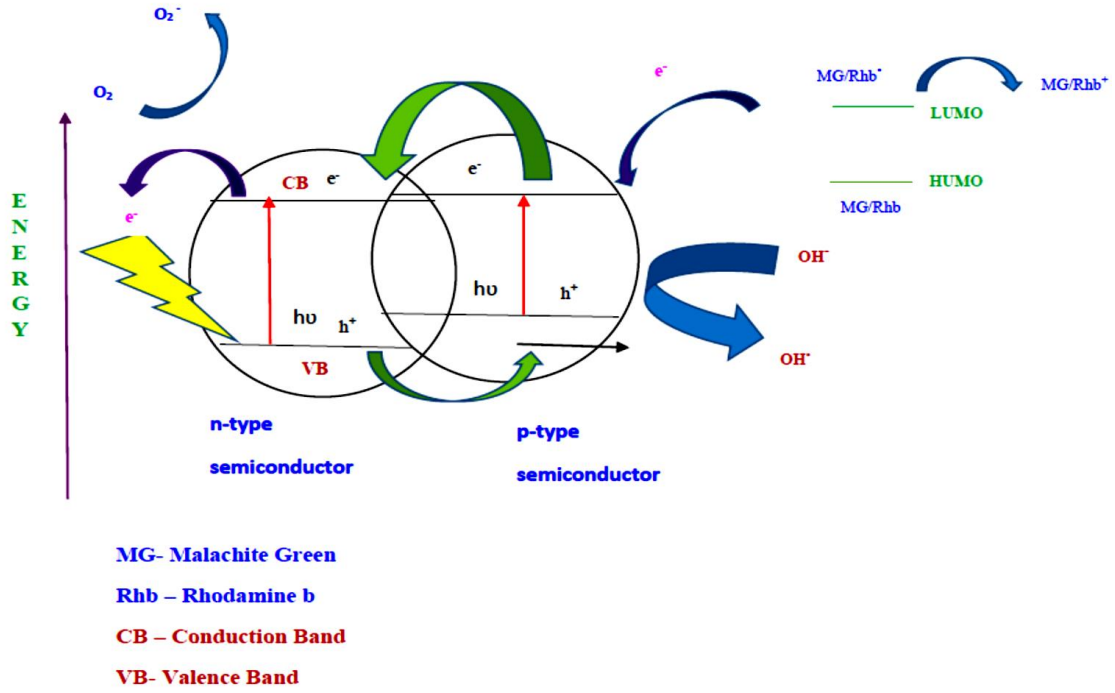

Figure 1: Schematic photophysical and photochemical processes over photon activated binary semiconductor nanocomposite.

1.3: Basic principles/Mechanism of photocatalysis

Photocatalytic reaction is initiated when a photo excited electron is promoted from the filled valence band of semiconductor photocatalyst (SC) to the empty conduction band as the absorbed photon energy hv, equals or exceeds the band gap of the semiconductor photocatalyst leaving behind a hole in the valence band. Thus in concert, electron and hole pair (e^- -h^+) is generated.[24] The following chain reactions have been widely postulated.

Photo oxidation: $SC + h\nu \longrightarrow e^- + H^+$ (1)

Oxygen ion sorption: $(\boldsymbol{O_2})_{ads} + e^- \longrightarrow \boldsymbol{O_2^-}$ (2)

Ionization of water: $H_2O \longrightarrow \boldsymbol{OH^-} + \boldsymbol{H^+}$ (3)

Protonation of superoxide: $\boldsymbol{O_2^-} + \boldsymbol{H^+} \longrightarrow \boldsymbol{OOH}\cdot$ (4)

The hydroperoxyl radical formed in (4) also has scavenging property as O_2 thus doubly prolonging the lifetime of photo hole:

$$\boldsymbol{OOH}^{\cdot} + e^{-} \longrightarrow HO_2$$

$$\boldsymbol{OOH}^{-} + H^{+} \longrightarrow \boldsymbol{H_2O_2}$$

Both the oxidation and reduction can take place at the surface of the photo excited semiconductor photocatalyst (Fig. 1). Recombination between electron and hole occurs unless oxygen is available to scavenge the electrons to form superoxide ($O_2^{\bullet-}$), its protonated form the hydroperoxyl radical ($HO_2^{\bullet}$) and subsequently H_2O_2.[25]

Heterogeneous photocatalysis is a discipline which includes a large variety of reactions: organic synthesis, water splitting, photo reduction, hydrogen transfer, O_2^{18}–O_2^{16} and deuterium–alkane isotopic exchange, metal deposition, disinfection and anti-cancer therapy, water detoxification. Among AOPs, heterogeneous photocatalysis has proved to be of real interest as efficient tool for degrading both aquatic and atmospheric organic contaminants. [26] Heterogeneous photocatalysis involve the acceleration of photoreaction in presence of semiconductor photocatalyst. One of the major applications of heterogeneous catalysis is photocatalytic oxidation (PCO) to effect partial or total mineralization of gas phase or liquid phase contaminants benign substances.[27] It is believed that the process of photocatalysis includes multiple reactions involving photochemical, chemical, electrochemical reactions etc. Despite many applications the basic photophysical principle and physical chemistry in photocatalysis is largely the same. Thus heterogeneous photocatalysis becomes an elegant alternative for dye degradation.TiO_2,ZnO, MgO,SiO_2,Cu_2O,CuO,WO_3,Fe_2O_3,ZrO_2[28] etc. are some of the metal oxides used for photocatalytic degradation of most common dyes like malachite green, rhodamanie-b, methyl orange etc.

1.4: Malachite Green

(4-{[4-(dimethyl amino) phenyl](phenyl)methylidene}-N,N-dimethylcyclohexa-2,5-dien-1-iminium chloride)

Malachite green (MG) (Basic Green 4; CI 42000) is widely used as a dye in the silk, wood, cotton, leather, paper, and acrylic industries[29] and also in the aquaculture industry as a biocide to control external fungal and protozoan infections of fish[30] [31] (Saha et al.,2012; Lee and Kim, 2012; Moumeni and Hamdaoui, 2012). The chemical structure of this MG dye is shown in Fig. MG has an aromatic complex molecular structure defiant to degradation and can reduce the transmission of sunlight to water bodies, thereby affecting the aquatic biota of the habitat. Hence,

MG will produce irreversible damage to the environment if discharged into water. Recently, MG has been listed as a priority chemical for carcinogenicity assessment by the U.S. Food and Drug Administration (Srivastava et al., 2004; Shedbalkar and Jadhav, 2011). Nonetheless, MG is still utilized in many regions worldwide due to its low cost, good efficacy, and a lack of suitable alternatives (Srivastava et al., 2004; Shedbalkar and Jadhav, 2011) Malachite green is environmentally persistent[32] and acutely toxic to a wide range of aquatic and terrestrial animals.[33] It causes serious public health hazards and also poses potential environmental problem. Both clinical and experimental observations reported so far reveal that malachite green is a multi-organ toxin.[34]

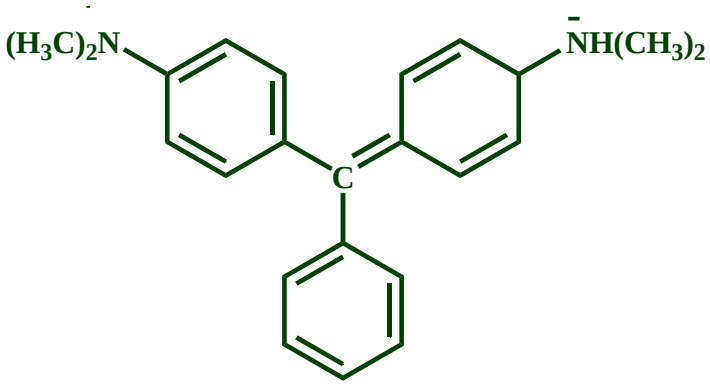

Figure 2: Chemical structure of malachite green

Mechanism of degradation of malachite green

The complexity of the degradation process is caused by the multiple sites prone to OH radical attack on malachite green(MG) and its byproducts in aqueous solution (Oturan et al., 2008), and generally, the generation of a carbon-centered radical is succeeded by the destruction of dye chromophore structures (Chen et al., 2007). A tentative mechanism for photocatalytic degradation of malachite green dye is proposed as follows:

$$^{1}MG_{0} \xrightarrow{h\nu} {}^{1}MG_{1}$$

$$^{1}MG_{1} \xrightarrow{ISC} {}^{3}MG_{1}$$

$$SC \xrightarrow{h\nu} e^{-}(CB) + h^{+}(VB)$$

$$^{-}OH + h^{+} \longrightarrow {}^{\bullet}OH$$

Malachite green (MG), on absorption of radiations of desired wavelength, is excited resulting in first excited singlet state.[35] Further, it undergoes intersystem crossing (ISC) to give its more stable triplet state. Simultaneously, the semiconducting nanocomposite (SC) also utilizes this energy to excite its electron from valence band to the conduction band. An electron can be abstracted from hydroxyl ion by the hole (h^+) present in the valence band of semiconductor generating OH radical. This hydroxyl radical will oxidize malachite green to its leuco form, which may ultimately degrade to products.[36] [37]

$$^{\bullet}OH + {}^{3}MG_1 \longrightarrow \text{Leuco MG}$$

$$\text{Leuco MG} \longrightarrow \text{Products}$$

1.5: Rhodamine-B

((*N-[9-(2-Carboxyphenyl)-6-diethylamino-3Hxanthen-3-ylidene]-N-ethyl ethanaminium chloride*)

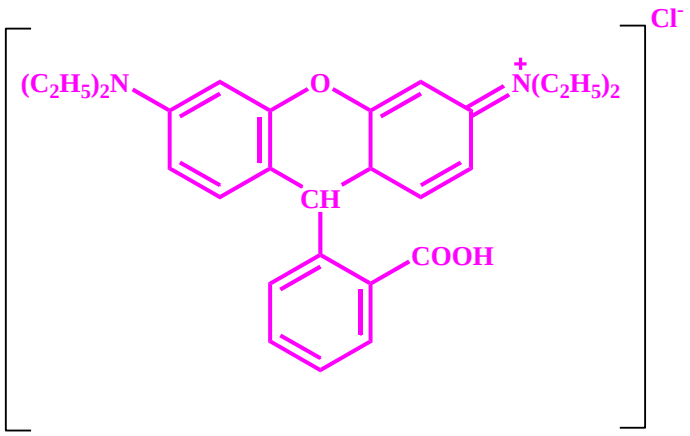

Figure 3 : Chemical structure of rhodamine B

Rhodamine B is one of the most common toxic dyes. The organic molecule absorbs visible light photons, which, whilst having insufficient energy to promote semiconducting (SC) metal oxide nanocomposite photo-activation, can promote electrons from the highest occupied molecular orbital (HOMO) to the lowest unoccupied molecular orbital (LUMO) in the organic molecule. These electrons are further injected from the Rh-B LUMO to the conduction band of SC-metal oxide nanocomposite, leading to the formation of Rh-B $^{+\bullet}$ molecular ion radicals. The transfer of the conduction band electron to adsorbed oxygen on the metal oxide surface produces $O_2^{-\bullet}$. Both radical species arising from this process are highly reactive leading ultimately to complete mineralization of the organic molecule.

1.6: Binary metal oxides as photocatalyst:

Binary metal oxides are potentially useful photocatalysts. These catalysts seem to be potentially promising, because binary oxide catalysts often exhibit higher catalytic activity and selectivity than what one can predict from the properties of their components. Introduction of bimetal oxides also increases the band gap energy between valence band and conduction, hence results in the prevention of recombination of holes and electrons.[10c] Recently, there are various studies on photocatalytic activities of coupled semiconductor photocatalysts, for example, TiO_2-WO_3[38] TiO_2-CeO_2,[38b] TiO_2-ZnO,[39] SiO_2-TiO_2,[40 41] ZnO-SnO_2,[42] In_2O_3-TiO_2,[43] TiO_2-Fe_2O_3 [44]etc. These coupled semiconductor photocatalysts may improve the photocatalytic efficiency by increasing the charge separation and range of photo absorption. In the meantime, their physical and optical properties are significantly changed, as a p-type semiconductor, CuO acts as a sink for photogenerated electrons. Since the photogenerated electrons move in the opposite direction, they can be accumulated in the valence band of the n-type semiconductor molecule and increase the efficiency of charge separation. Copper oxide is a semiconductor material and has a natural abundance of starting material (Cu). It is non-toxic and easily obtained by the oxidation of Cu. Copper oxide is one of the important metal oxide which has attracted recent research because of its low cost, abundant availably as well as its peculiar properties. It is used in the fields like catalysis, superconductors, ceramics as a kind of important inorganic materials etc., CuO has been used as a basic material in cuprate high-T_c superconductors as the superconductivity in these classes of systems is associated with Cu-O bonding.[45] Among all metal oxide nanoparticles, copper oxide has gained the most interest because of its wide applications, such as in solar cell technology, field emission, magnetic storage media, lithium ion batteries, gas sensing, drug delivery, magnetic resonance imaging, and field emission devices. Varieties of physical and chemical methods have been proposed to synthesize CuO nanoparticles(CuO-NPs).[46] CuO-NPs belong to monoclinic structure system with the brownish-black appearance. [47] In perspection of these properties, the coupling of CuO and the n-sort semiconductor SnO_2 enhances their photocatalytic movement. Preparation of CuO NPs involves sol gel technique. The aim of this study was to advance the arrangement for the CuO-SnO_2 photocatalysts and investigate their photocatalytic activities. For this reason, a progression of nanosized CuO-SnO_2 photocatalysts with different calcination temperatures and different molar degree of Cu to Sn

were arranged and their photocatalytic exercises were assessed with malachite green and rhodamine-b as a model natural compound.

1.7: Knowledge gap

In the above section, the uses of metal oxide for photocatalytic degradation study are outlined. Though some progress has been made in these directions, still a lot need to be addressed for the use of binary metal oxide for photocatalytic degradation of toxic dyes.

- In the traditional photocatalyst such as TiO_2, ZnO, CuO and SnO_2, there is high degree of probability of recombination of valence shell and conduction shell band of electron-hole pair carriers which decrease greatly their photocatalytic efficiency. So keeping this in mind we have decided to synthesize p–n type hetero- structure SnO_2-CuO novel nanocomposite. This is a new system for photodegradation which has not been studied.
- Reason for selection for SnO_2-CuO nanocomposite: the valence band (VB) level of CuO semiconductor is lower than that of SnO_2 semiconductor. So, the holes generated in the VB of CuO semiconductor can be transferred to that of SnO_2 semiconductor after interaction with UV radiation. As a result, the separation and migration of photogenerated carriers can be promoted by the internal field, so less of a barrier exists. Therefore, the probability of electron–hole recombination can be reduced. A larger number of electrons on the CuO semiconductor surface and holes on the SnO_2 semiconductor surface can be generated, respectively, which participate in the photodegradation process to directly or indirectly degrade organic pollution, and thus the photocatalytic reaction can be enhanced greatly.

1.8: Objectives of the present study:

- To synthesize, SnO_2 nanoparticle, CuO nanoparticle and SnO_2-CuO binary composite by sol-gel method.
- To find out the optimize concentration ratio of photocatalyst by varying both the salt loading ratio such as (1:1, 2:1, 1:2, 1:0.5, 0.5,1,for pure SnO_2 and pure CuO respectively).
- To characterize binary metal oxide using UV-Vis, SEM/EDX, XRD, TGA and PL spectra.
- Catalytic activity of prepared catalysts calcined at different temperature (400 °C, 500 °C and 700 °C) will be studied for photocatalytic degradation of methylene blue under visible light.

CHAPTER 2: EXPERIMENTAL

2.1: Material Used

All chemicals are analytical grade and used as purchased without further purification.Tin chloride dihydrate (Sigma Aldrich), Copper nitrate hexahydrate (Merck), Ammonia (Rankem), malachite green and Rhodamine B dyes (purchased from local firm).

2.2: Synthesis of SnO_2 and CuO nanoparticle

For synthesis of SnO_2 nanoparticle, 1.5 g of $SnCl_2.2H_2O$ was first dissolved in 50 ml water. After complete dissolution, 3.5 ml of ammonia solution was added dropwise. The contents were stirred for 15 min at room. The resulting gels were filtered and dried at 80 ^{0}C for 24 hrs.in order to remove water molecules. Finally, tin oxide nanopowder was calcined at 700 ^{0}C for 2hrs.CuO nanoparticle by similar procedure using Cu $(NO_3)_2.3H_2O$ precursor.

2.3: Synthesis of SnO_2-CuO nanocomposite

For synthesis of SnO_2-CuO nanocomposite, 1.5 g of $SnCl_2.2H_2O$ was first dissolved in 50 ml water. Then 3.5 ml of ammonia solution was added dropwise. The contents were stirred for 15 min at room temperature. After than appropriate amount of Cu $(NO_3)_2.3H_2O$ were initially dissolved in 20 ml of water and transferred to an autoclave. The solution was allowed to reach to 180 °C within 1 hour. The reaction was kept at this temperature for 8 hours. After 8 hours, it was cooled to room temperature. The product was filtered, washed with water and ethanol many times to remove the chloride ions and other impurities. The obtained product was dried at 80 °C in a hot air oven for overnight. The final product was pale green in color. Finally, nanopowders were calcined at 700^{0}C for 2hrs.

2.4: Photocatalysis

2.4.1: Characterization

The catalyst was analyzed by X-Ray diffraction study using PHILIPS PW 1830 X-ray diffractometer with CuK_α source. The compositional information of the products was performed

using EDX (JEOL JSM-6480 LV). Field emission scanning electron microscopy (FESEM) of the sample was recorded by Nova Nano SEM/FEI

2.4.2: Instrumentation

Photocatalytic studies were conducted in a dark reaction chamber (50 cm x 50 cm x 50 cm) and an artificial sunlight setup was used. The source of light used for visible radiation was a Bajaj, high pressure mercury vapour (HPMV) lamp, 125W, 220-250V with peak emission at a wavelength of about 450 nm. The distance between the lamp and the surface of the solution was about 15cm.

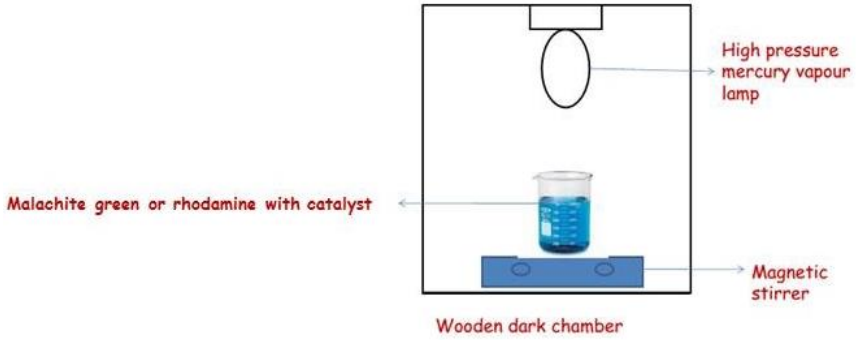

Figure 4: Photocatalytic set-up

2.4.3: Photocatalytic Measurements

The photocatalytic activity was evaluated by the degradation of Malachite Green (MG) and Rhodamine-B (RhB), respectively. In a typical process, 0.04 gas-fabricated materials were suspended in 200 ml malachite green and Rhodamine solution (20 mg l^{-1}). The suspensions were magnetically stirred in the dark to ensure an adsorption/desorption equilibrium, and the solution was then exposed to an UV lamp at room temperature. At given irradiation time intervals, the samples were collected regularly to measure the degradation of dyes by UV-vis spectroscopy.

CHAPTER 3: RESULTS AND DISCUSSION

3.1: Characterization of the SnO_2-CuO nanocomposite

3.1.1: TGA-DTA

TG-DTA was carried out to determine a suitable calcination temperature of SnO_2-CuO (1:1) nanocomposite. The TGA curve of Fig. 5 shows a weight loss. In the range of temperature less than 200 (<200) is due to presence of adsorbed water. The weight loss occurring between 250 ℃ and 600 °C, the organics belonged to nitrate group of copper nitrate and some volatile tin species such as chloride composites evaporate.

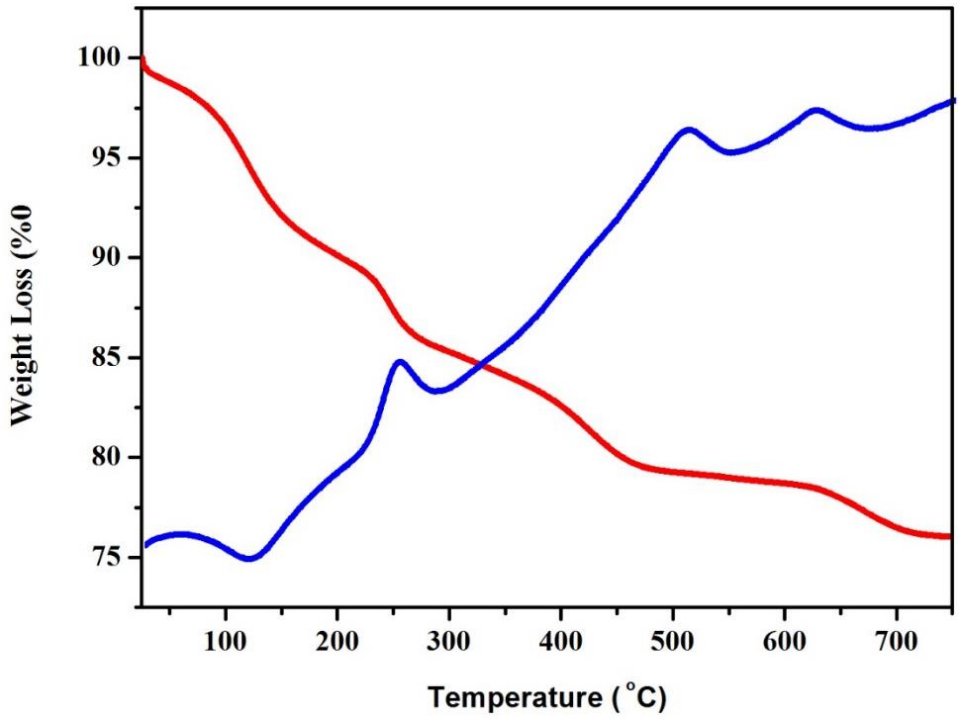

Figure 5: Thermal profiles obtained from TG-DTA for SnO_2-CuO (1:1) nanocomposite

The DTA curve of the SnO_2-CuO nanocomposite reveals that semiconductor characteristics are present only after annealing at temperatures above 575°C, because below this temperature, both solvent and organic molecule residues can act as obstacles for charge carrier accumulation and transportation in the conduction band. The phase transformation from amorphous to crystalline states also occurs at this temperature. It should be noted that there was no change in weight loss above 650°C, revealing that a calcination temperature of 650 °C is needed to remove the solvent and to fully decompose zinc acetate and tin chloride into a pure SnO_2-CuO phase.

3.1.2: XRD Analysis

XRD was used to investigate the phase structures and average crystallite size of the uO-SnO_2 nanocomposite as a photocatalystpowders.Fig.6 shows the XRD patterns of the CuO-SnO_2 photocatalyst powders calcined at different temperatures (400°C, 500°C and 700°C, 3 h). Good crystalline peaks were observed for 700 ^{0}C with 2Θ values 26.55°, 33.82°, 35.58°, 38.53°, 48.66°, 51.61°, 54.47°, 58.24°, 61.56°, 65.52°, 68.00° consistent with (110), (020),(101), (022) ,(111), (202), (211), (220), (113), (022) and (311) spacing's respectively (JCPDS card file no: 88-0287).

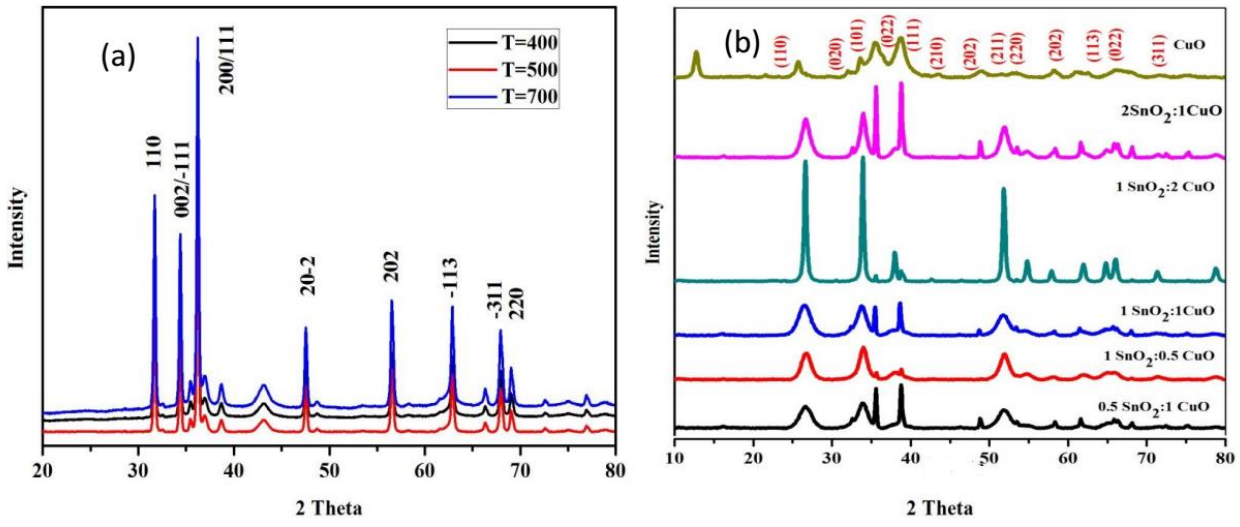

Figure 6: a) XRD patterns of the CuO-SnO2 photocatalyst calcined at different temperature and b) Different composition of [Sn^{4+}]: [Cu^{2+}] salt

It can be seen that the prepared sample at low temperature (400°C) shows such weaker

crystallization that only SnO_2 can be observed. While calcined at 500°C for 3 h, the diffraction peaks of the sample can be indexed with the SnO_2 and CuO phase of the CuO-SnO_2 photocatalyst powders. With the increase of calcination temperature (at 700°C), no other new peaks could be detected except for the SnO_2 and CuO phases, but the diffraction peak intensity of the CuO-SnO_2 photocatalyst powders obviously increases and the width of the peak is gradually narrower. For the samples calcined at 400–700°C, an average particle size of around 50–150 nm was estimated by applying the Scherrer equation on the highest intensity diffraction peaks of SnO_2. X-ray structure analysis for the CuO-SnO_2 photocatalyst also illuminated that the CuO and SnO_2in the coupled CuO-SnO_2 photocatalyst exist in the form of a physical mixture, but not a core shell type. It can be seen that the CuO-SnO_2 photocatalyst powders calcined at 400°C appeared amorphous in nature. By contrast, the CuO-SnO_2 photocatalyst powders calcined at 700°C displayed greater particle size (about 60 nm) due to sintering between smaller particles. Increase of the heat treatment temperature caused CuO-SnO_2 photocatalyst particles become larger.

3.1.3: UV-Vis

Figure.7. gives the UV-Vis diffuse absorbance spectra of the CuO-SnO_2 photocatalyst powders of different ratio such as 1:1,1:2,2:1,1:0.5 and 0.5:1 calcined 700°C. From the UV spectra it implies that the absorption edge of the CuO-SnO_2 catalyst shifts towards the longer wavelength range.

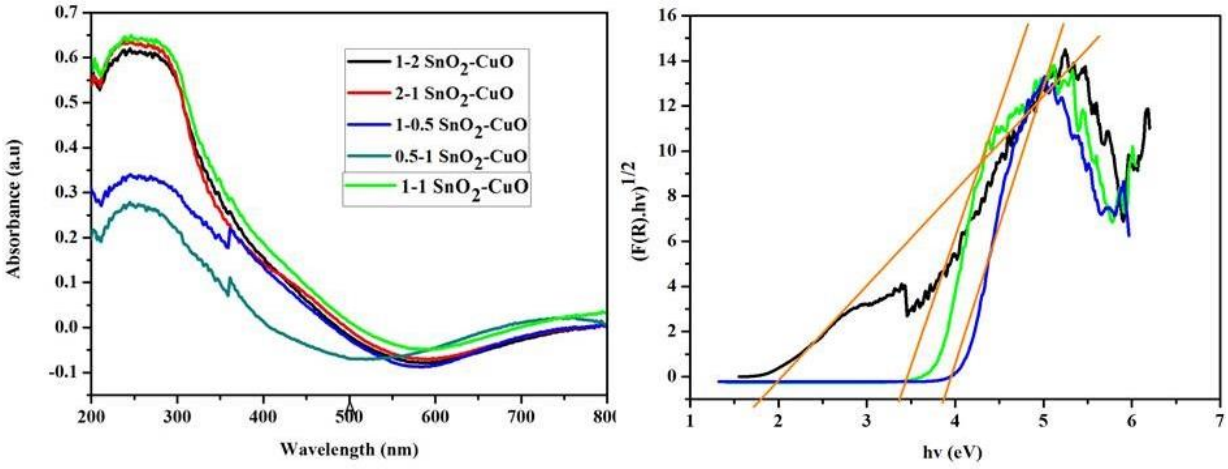

Figure 7: UV-vis spectra of SnO_2–CuO nanocomposites after calcination at 700 ^oC and estimation of band gap of SnO_2–CuO nanocomposite, pure SnO_2, pure CuO nanoparticles.

The bandgap energies of the photocatalysts were determined from the Tauc plot, a plot between $(F(R).hv)^{1/2}$ versus hv. F(R) is the Kubelka–Munk function derived from reflectance spectra where $F(R) = (1-R)^2/2R$ equation and hv is the photon energy. On doping with metal oxide nanoparticles the bandgap decreases and shifts the wavelength toward the lower energy region. Bandgap of pure SnO_2 nanoparticle and CuO nanoparticles were calculated to be 3.28eV and 1.7 eV. While mixing both metal oxides to form SnO_2-CuO binary nanocomposite, the bandgap decreases and shifts to lower energy side. The band gap of as synthesized 1:1 ratio of SnO_2-CuO comes around 3.2eV. Tauc's plot for pure SnO_2, pure CuO and SnO_2-CuO is shown in Fig.7.

3.1.4: FESEM/EDX

The detailed morphology and microstructure of the pure SnO_2 nanoparticle, pure CuO nanoparticle and SnO_2-CuO heterojunctions nanocomposite concentrations (1:1) were inspected by FESEM. The morphology of the pure SnO_2 nanoparticle appears to be irregular aggregates with size ranging between 100 and 500 nm (Figure 8a). The pure CuO nanoparticle

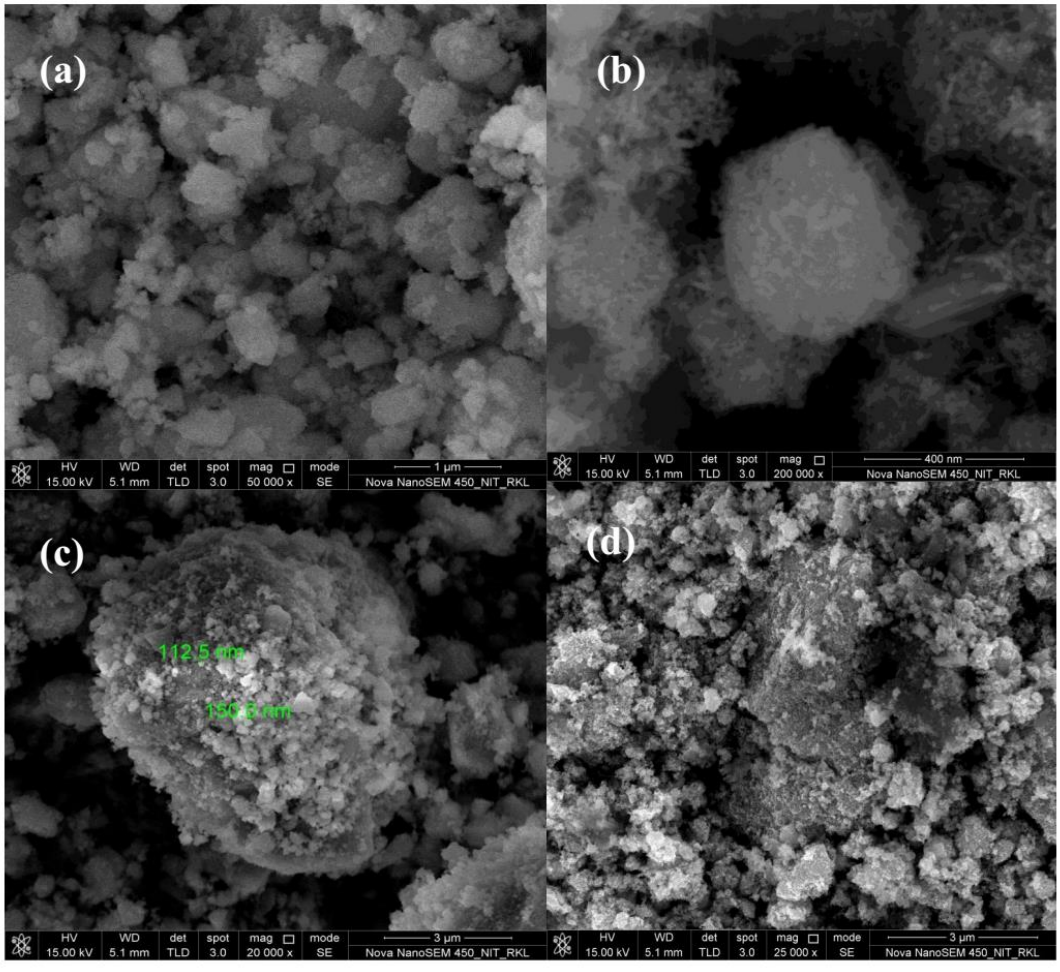

Figure 8: SEM photomicrographs of (a) SnO_2 nanoparticle, (b) CuO nanoparticle and (c-d) SnO_2-CuO nanocomposite

consists of a large quantity of irregular rod shape structure with smooth surface which are in the range of nanometer to micrometer in size. The morphology of the SnO_2-CuO heterojunctions nanocomposite is shown in Figure 8c-d. From the Fig. we can see homogeneous spherical shape metal oxide nanocomposite which are uniformly mixed. Therefore, we conclude that morphologies of all the heterojunctions exhibit the coexistence of SnO_2 and CuO metal oxide. No other morphologies are observed in the FESEM images which indicate the purity of the products. The contact between SnO_2 nanoparticles and CuO nanoparticle is observed to be good at all the heterojunctions, facilitating the interparticle electron transfer between SnO_2 and CuO.

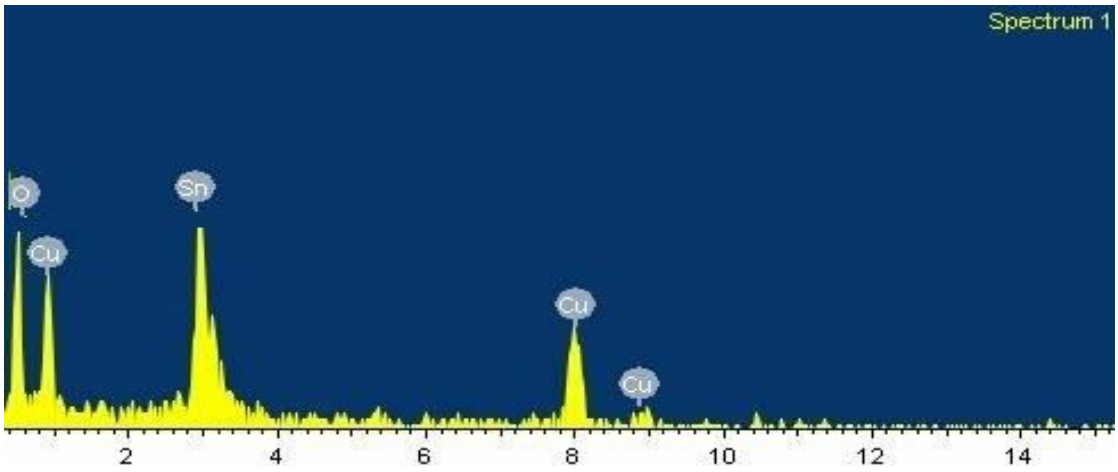

Figure 9: EDX spectrum of SnO_2-CuO nanocomposites.

The Energy dispersive X-ray Diffractive (EDX) study was carried out for the synthesized SnO_2-CuO nanocomposite (Figure 9) to know about the elemental composition. EDX confirms the presence of element tin, copper and oxygen signals of nanocomposite and this analysis showed the peaks that corresponded to the optical absorption of the produced nanocomposite. The elemental analysis of the nanocomposite yielded 50% of tin and 50% of copper which proves that the produced nanocomposite is in its highest purified form.

3.1.5: Photoluminescence

The photoluminescence spectra of the as-synthesized SnO_2-CuO nanocomposite. In the SnO_2-CuO nanocomposite there are two strong emissions corresponding to 416 and 462nm along with few weak bands observed at 478,488 and 502 nm, and a broad band at 557 nm respectively. Since the position of the emission maxima are lower than the respective band gap of the SnO_2,

these emission cannot be attributed to the direct recombination of a conduction electron in the Sn 4p band and a hole in the O 2p valence band. Therefore, these emissions may be attributed to the different luminescent centers such as defect energy levels arising due to tin interstitials and oxygen vacancies as well as dangling bonds into nanocrystals. The V^{0}_{O} ,V^{+}_{O} and V^{++}_{O} are the most common defects arising due to oxygen vacancies and trap electrons from the valence band, and may act as luminescent centers inside the bandgap. The emissions in the broad visible range around 400 to 500 nm are due to formation of the doubly ionized oxygen vacancies. When the

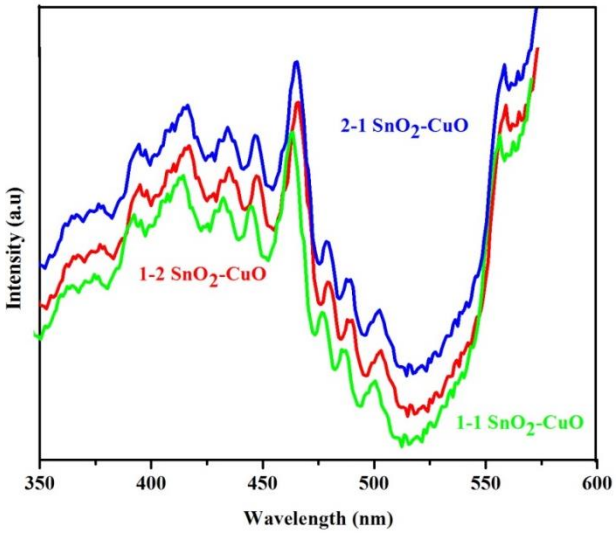

Figure 10: Photoluminescence spectra of SnO_2-CuO nanocomposite of different composition

sample is exposed to UV radiation (248 nm) , electron is excited from the valence band to the conduction band, leaving a hole in valence band. The recombination of this active hole with an electron in deep trap (V^{+}_{O}) forms V^{++} O center which gives rise to visible emission when a conduction band electron recombines with the $V^{++}O$ center. Normally, the most common emission bands observed and coexist in SnO_2 are green and red/orange, which are attributed to the deep traps forming defects energy levels inside the SnO_2 band gap. It has been observed that the intensity of emission bands decreases with the increasing Cu doping concentration in the SnO_2 matrix. This could be attributed to a concentration quenching effect characterized by the energy exchange between a pair of Cu ions. This non radiative process is generally described by a cross-relaxation process in which two neighboring ions exchange energy and by the migration of the excitation energy.

3.2: Photocatalytic studies

3.2.1: Photocatalytic behaviour of malachite green and rhodamine B

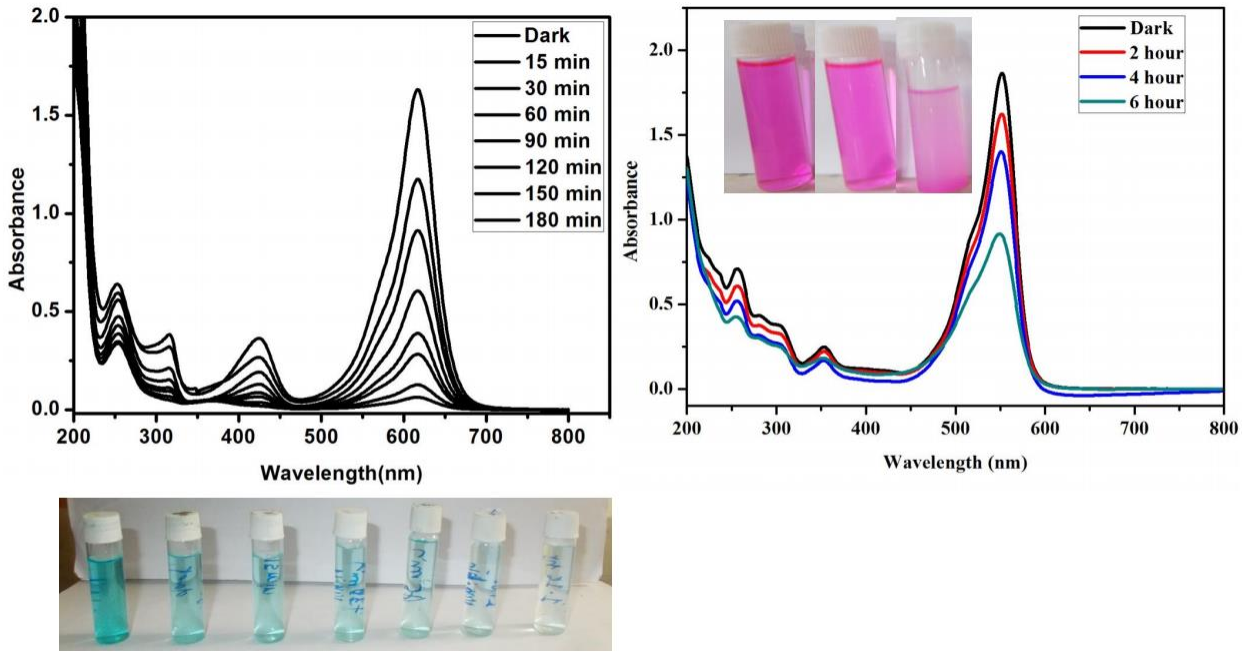

Figure 11: Photocatalytic degradation of (a) malachite green and (b) rhodamine B over SnO_2-CuO (1:1) nanocomposite

The UV-Vis spectra of MG and RhB degradation process at different time intervals using SnO_2-CuO (1:1 ratio) nanocomposite was given in Fig.11. SnO_2-CuO nanocomposite shows much faster and higher degradation rate for malachite green dye as compare to rhodamine b dye. After 180 min it was observed that SnO_2-CuO nanocomposite shows around 96 % of degradation, whereas for rhodamine B dye same catalyst show 49% degradation in 6 hours. Both the degradation study was done in UV irradiation.

3.2.2: Photodegradation of MG and RhB with various catalysts

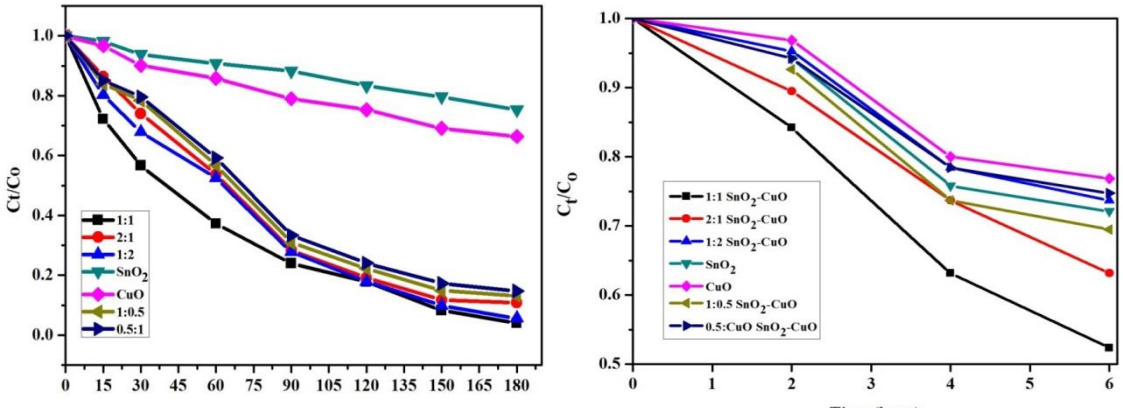

A blank reaction carried out in the absence of the catalyst also indicates that the efficiency is not good. Fig.12 shows the kinetics of degradation of malachite green and rhodamine B dyes using different SnO_2–CuO nanoparticles. It can be noticed that the SnO_2– CuO nanoparticles prepared using $[Sn^{4+}]$: $[Cu^{2+}]$ = 1:1 shows the fastest degradation among all the synthesized mixed metal oxide nanoparticles.

3.2.3: Influence of catalyst loading

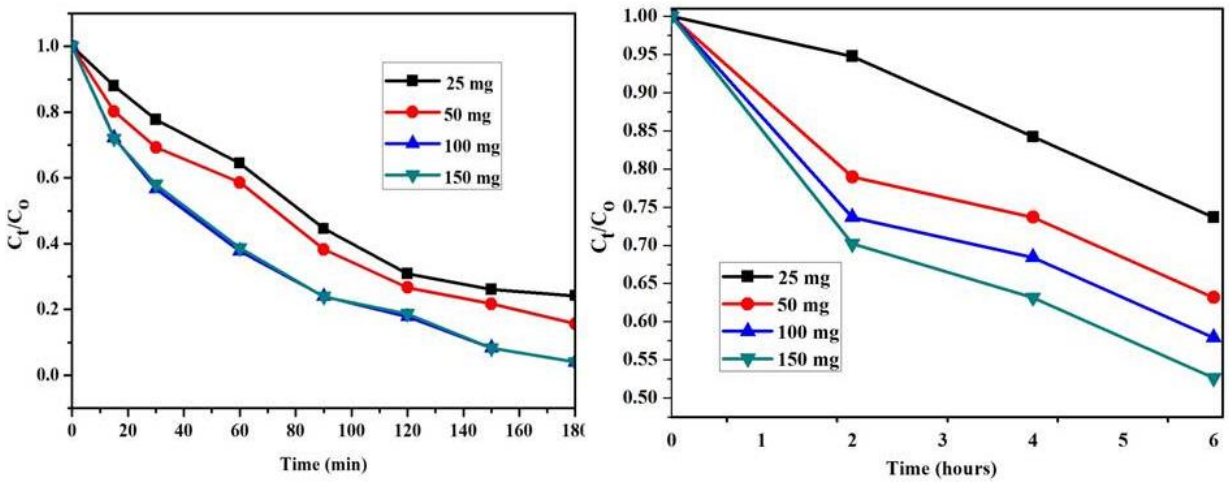

Figure 13: Photocatalytic degradation of (a) malachite green and (b) rhodamine b dyes at different catalyst loading

To enhance the measure of photocatalyst, a progression of analysis were done by differing the catalyst measurements from 25 mg to 150 mg with dye concentration of 20 ppm and the outcomes are demonstrated in the Fig.13.The plot investigates that when the catalyst amount was expanded from 25 mg to 100 mg, the degradation process increases. With the increment in catalyst amount, the quantity of active sites increases on the catalyst surface bringing about the adsorption of more dye particles. Thus, the photocatalytic degradation increases. The catalyst measure of 100 mg was discovered to be an ideal amount for the degradation study. In the meantime, the more prominent measure of photocatalyst makes a relating increment in number of dynamic radicals by absorbing higher measure of photons, making degradation less difficult,

especially for the adjacent dye atoms. However, the effect of photocatalyst has a tendency to decreasing when the catalyst amount was higher than 100 mg. higher measure of catalyst concentration applies additionally scattering for which the entrance intensity of light illumination lessened. Thus, the perfect measure of photocatalyst was 100 mg with dye concentration 20 ppm. In this work, every single other examination were done by taking 100 mg as the ideal catalyst measurements.

Similarly for Rhodamine b dye the catalyst amount was varied and 150mg catalyst amount was varied as optimal catalyst dose.

3.2.4: Kinetic study

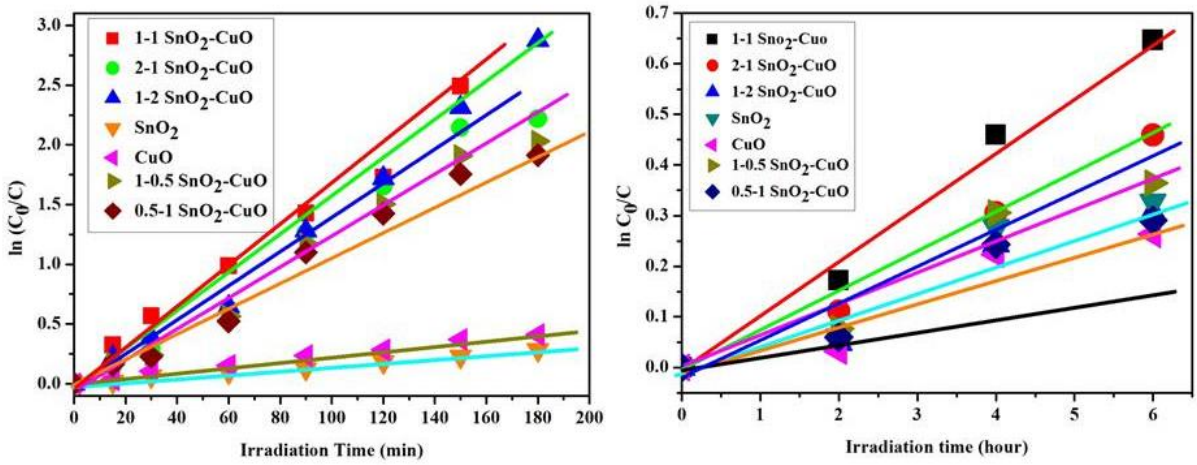

Figure 14: Pseudo- first- order kinetics plot of (a) malachite green and (b) rhodamine b dyes degradation over pure SnO_2, pure CuO and SnO_2-CuO nanocomposite.

The kinetics of these morphologies of SnO_2-CuO for the degradation of malachite green and rhodamine B was studied and it was found that the degradation reactions of all the different composition with MG and RhB showed pseudo-first-order kinetics for specific time of degradation. All the obtained kinetics information agrees fully with the linear equation.

$$\ln\left(\frac{C_o}{C_t}\right) = -kt$$

Here C_0 is the initial concentration of dyes and C is the concentration at interval of time t, k is specific rate constant for the first order kinetics reaction. For the first order kinetics, a graph

between the values of $\ln(C_o/C)$ versus time for the degradation of malachite green and rhodamine B is plotted using SnO_2-CuO nanocomposite as shown in Fig.14 illustrates a linear correlation and it indicates that the malachite green and rhodamine B degradation.

3.2.5: Mechanism for the photodegradation

Under UV light irradiation, electrons in the valence band of SnO_2 are excited to conduction band with the same amount of holes left behind in the valence band. The photogenerated holes and electrons tend to recombine but in the presence of CuO, the electrons in the conduction band of SnO_2 transfer to that of CuO (Fig. 15). Consequently, the photogenerated holes and electrons are separated at the interface of the SnO_2–CuO nanocomposite. The SnO_2–CuO nanocomposite prepared using [Sn^{4+} :Mg^{2+}] = 1:1 show the best efficiency for the degradation of malachite green and rhodamine B compared to pure SnO_2 and pure CuO samples.

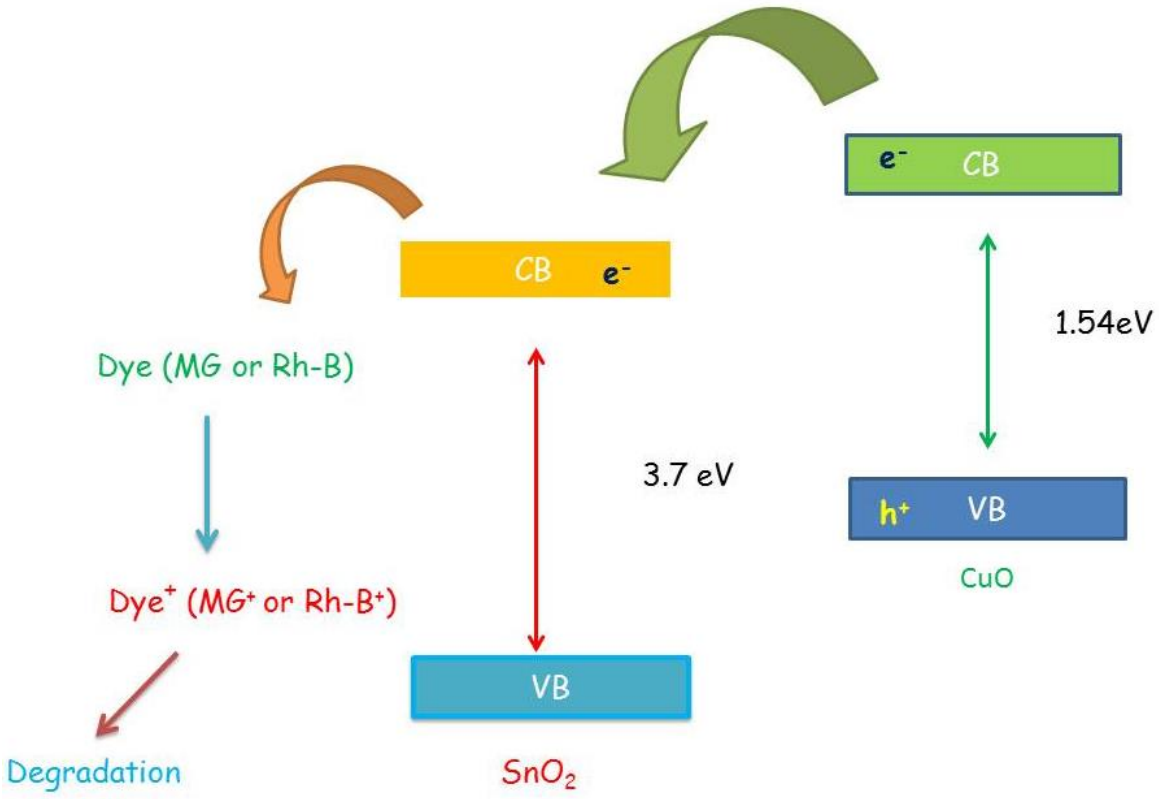

Figure 15: Schematic diagram showing the electron-hole separation at the interface of SnO_2-CuO nanocomposite

3.2.6: Recyclability

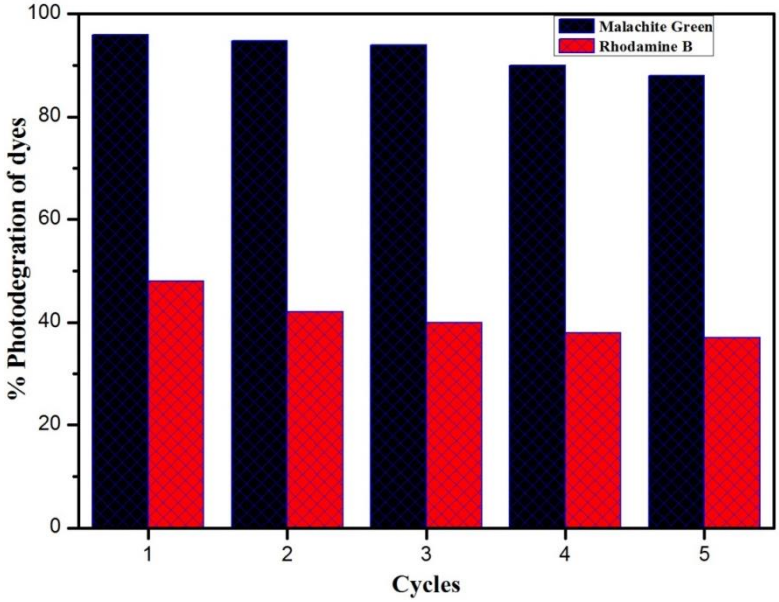

Figure 16: Recycling experiments for the degradation of (a) malachite green and (b) rhodamine B dyes SnO_2-CuO (1:1) nanocomposite.

To make the process cost-effective and greener, the recycle ability of SnO_2-CuO nanocomposite toward photocatalytic behavior toward malachite green and Rhodamine B dyes was evaluated. The efficiency decreased slightly as the catalyst was reused for many times. After completion of one catalytic cycle, prior to reuse, the used SnO_2-CuO nanocomposite were collected by centrifugation, washed with water and ethanol for three times each and dried at 110 ^{0}C in an oven for 2 h, and reused for a fresh batch of MG solution and RhB dyes.

CHAPTER 4: Conclusions

- A Novel CuO-SnO_2 nanocomposite was prepared via a simple sol-gel method.
- Their phase compositions and photocatalytic activities were studied with regard to the calcination temperature and the molar ratio of Cu to Sn. The CuO-SnO_2 photocatalyst calcined at 700 °C for 2h (the molar ratio of Cu to Sn is 1:1) was found to show the best photocatalytic activity due to the sample with good crystallinity.
- In comparison with SnO_2 and CuO nanoparticle, the CuO-SnO_2 photocatalyst showed higher photocatalytic activity. This higher photocatalytic behavior can be explained on the basis of synergetic effect on the specific adsorption property and efficient electron-hole separation at the CuO-SnO_2 photocatalyst interface.

FUTURE WORK

- Further study will be done on recyclability of the catalyst.
- In a sense, the effective photodegradation of dyes such as malachite green and rhodamine b by CuO-SnO_2 photocatalyst under UV irradiation is a very exciting respect in photocatalytic area, and this work may provide new insights into the development of novel sunlight photocatalysts.

CHAPTER 5: References

1. Gogate, P. R.; Pandit, A. B., *Adv. Environ. Res.* **2004,** *8*, 501-551.
2. Guillard, C.; Disdier, J.; Herrmann, J.-M.; Lehaut, C.; Chopin, T.; Malato, S.; J. Blanco, *Catal. Today* **1999,** *54*, 217-228.
3. T. Kudo, Y. N., A. Ruike, *Res. Chem. Intermed.* **2003,** *29*, 631.
4. Carp, O.; Huisman, C. L.; Reller, A., *Prog. Solid State Chem.* **2004,** *32*, 33-177.
5. Parsons, S., *IWA Publishing* **2004**.
6. M. Derudi, G. V., G. Lombardi, G. Nano, R. Rota, *European Journal of Soil Biology* **2007,** *43*, 297–303.
7. (a) M.J. Martin, A. A., M.D. Balaguer, M. Rigola, *Chemical Engineering Journal* **2003,** *94*, 231–239; (b) A.L. Ahmad, S. W. P., *Chemical Engineering Journal* **2007,** *132*, 257–265; (c) I. Arslan; I.A. Balcioglu; Bahnemann, D. W., *Dyes and Pigments* **2000,** *47*, 207–218; (d)] J.H. Mo, Y. H. L., J. Kim, J.Y. Jeong, J. Jegal, *Dyes and Pigments* **2008,** *76* 429–434; (e) M.A. Rauf, S. S. A., S.N. Alhadrami, *Dyes and Pigments* **2005,** *66*, 197–200.
8. Hoffmann, M. R.; Martin, S. T.; Choi, W.; Bahenemann, D. W., *Chem. Rev.* **1995,** *95*, 69-96.
9. (a) A.L. Pruden, D. F. O., *J. Catal.* **1983,** *82*, 404–417; (b) S. Irmak, E. K., O. Erbatur, *Appl. Catal. B: Environ.* **2004,** *54*, 85–91.
10. (a) Wang, Y., *Water Res.* **2000,** *34*, 990–994; (b) C. Bauer; P. Jacques; Kalt, A., *J. Photochem. Photobiol. A: Chem.* **2001,** *140*, 87–92; (c) M. Saquib, M. M., *Dyes Pigments* **2003,** *56*, 37–49; (d) I.K. Konstantinou, T. A. A., *Appl. Catal. B: Environ.* **2004,** *49*, 1–14.
11. (a) M. Muruganandham, M. S., *Sol. Energy Mater. Sol. Cells* **2004,** *81*, 315–321; (b) M. Muruganandham, M. S., *Dyes Pigments* **2004,** *63*, 315–321; (c) M. Muruganandham, M. S., *Dyes Pigments* **2004,** *62*, 269–275.

12. T.V. Gerven, G. M., J. Moulijn, A. Stankiewicz, *Chem. Eng. Proc.* **2007,** *46*, 781–789.
13. Yin, S.; Ihara, K.; Komatsu, M.; Zhang, Q.; Saito, F.; Kyotani, T.; Sato, T., *Solid State Comm.* **2006,** *137*, 132-137.
14. B. G. Mishra, G. R. R., *J. Mol. Catal. A: Chem.* **2006,** *243* 204.
15. D. Kumar, B. G. M., V. Buchi Reddy, R.K. Rana, R.S. Varma, *Tetrahedron* **2007,** *63*, 3093.
16. Zhao, J.; Yang, X., *Build. Environ.* **2003,** *38*, 645-654.
17. Minero, C.; Vione, D., *Appl. Catal. B: Environ.* **2006,** *67*, 257-269.
18. Serpone, N.; Lawless, D.; Khairutdinov, R.; Pelizzetti, E., *J. Phys. Chem. B* **1995,** *99*, 16655-16661.
19. (a) S.N. Frank, A. J. B., *J. Am. Chem. Soc.* **1977,** *99*, 303; (b) S.N. Frank, A. J. B., *J. Phys. Chem.* **1977,** *81*, 1484.
20. (a) Heller, A., *Acc. Chem. Res.* **1995,** *28*, 503; (b) A. Fujishima, T. N. R., D.A. Tryk, *J. Photochem. Photobiol. C* **2000,** *1*, 1; (c) T. Watanabe, A. N., R. Wang, M. Minabe, S. Koizumi, A. Fujishima, K. Hashimoto, *Thin Solid Films* **1999,** *351*, 260.
21. (a) M. C. Lee, W. C., *J. Phys. Chem. B* **2002,** *106*, 11818; (b) Y. Ishikawa, Y. M., Y. Nishida, S. Taniguchi, J. Watanabe, *J. Am. Chem. Soc.* **2003,** *125*, 6558; (c) T. Tatsuma, W. K., A. Fujishima, *Langmuir* **2002,** *18*, 9632.
22. (a) ; (b) R. Gorges, S. M., G. Kreisel, *J. Photochem. Photobiol. A: Chem* **2004,** *167*, 95; (c) K. Naoi, Y. O., T. Tatsuma, *J. Am. Chem. Soc.* **2004,** *126*, 3664; (d) K. Naoi, Y. O., T. Tatsuma, *Chem. Commun.* **2005**, 1288; (e) S. Teekateerawej, J. N., Y. Nosaka, *J. Photochem. Photobiol. A: Chem* **2006,** *179*, 263; (f) G. Takei, T. K., H.-B. Kim, *Catal. Commun.* **2005,** *6*, 357; (g) E.T. Castellana, S. K., F. Albertorio, *Cremer, Anal. Chem.* **2006,** *78*, 107; (h) G. Takei, M. N., A. Hibara, T. Kitamori, H.-B. Kim, *Lab Chip* **2007,** *7*, 596.
23. H. Nagai, T. I., J. Takahashi, S.-i. Wakida, *Biosens. Bioelectr.* **2007,** *22*, 1968.
24. A. Fujishima, K. H., *Nature* **1972,** *238*, 37.
25. Kim, H.; Lee, S.; Han, Y.; Park, J., *J. Mater. Sci.* **2005,** *40*, 5295-5298.
26. Lawless, D.; Serpone, N., *J. Phys. Chem. B* **1991,** *95*, 5166-5170.
27. C. Guillard, J. D., J.-M. Herrmann, C. Lehaut, T. Chopin, S. Malato, J. Blanco, *Catal. Today* **1999,** *54*, 217.

28. W.A. Zeltner, D. T. T., *American Society of Heating and Air-Conditioning Engineers Inc.* **2005,** *2*, 532.
29. I.K. Konstantinou, V. A. S., T.A. Albanis, *Water Res.* **2002,** *36*, 2733.
30. (a) S.J. Culp, F. A. B., *J. Am. Coll. Toxicol.* **1996,** *15*, 219–238; (b) V. Adams, J. M., Br. Dent, *J. Occup. Environ. Med* **2007,** *203*, 585–591.
31. A.J. Linz, R. K. G., L.F. Fallon, *J. Occup. Environ. Med.* **2006,** *48*, 523–530.
32. S. Srivaji, R. S., D. Roy, *Aquat. Toxicol.* **2004,** *66*, 319–329.
33. Schnick, R. A., *Prog. Fish Cult.* **1998,** *50*, 190–196.
34. S. Srivaji, R. S., D. Roy, *Aquat. Toxicol.* **2004,** *66*, 319–329.
35. Sayılkan, F.; Asilturk, M.; Tatar, P.; Kiraz, N.; S¸ener, S.; Arpac, E.; Sayılkan, H., *J. Mater. Res. Bull.* **2008,** *43*, 127-134.
36. Chen, C. C.; Zhao, W.; Li, J. G.; Zhao, J. C.; Hidaka, H.; Serpone, N. *Environ. Sci.Technol.* **2002,** *36*, 3604-3611.
37. Kyung, H.; Lee, J.; Choi, W., *Environ. Sci. Technol.* **2005,** *39*, 2376–2382.
38. (a) Linsebigler, A. L.; Lu, G. Q.; Jr, J. T. Y., *Chem. Rev.* **1995,** *95*, 735–758; (b) Shiyanovskaya, I.; Hepel, M., *J. Electrochem. Soc.* **1999,** *146*, 243–249.
39. D. Camino, D. D., J. Salardenne, N. Treuil, *Sol. Energ. Mater. and Sol. Cells* **1995,** *39*, 349–366.
40. K. H. Yoon, J. C., D. H. Kang, *Mater. Res. Bull.* **1999,** *34*, 1451–1461.
41. Liu, R. J. D. a. Z., *Chem. Mater.* **1999,** *9*, 2311–2324.
42. Davis, Z. L. a. R. J., *J. Phys. Chem. B* **1994,** *98*, 1253–1261.
43. Wang, C.; Wang, X.; Xu, B. Q.; J.Zhao; Mai, B.; Peng, P. a.; Sheng, G.; Fu, J.; A. Fujishima; Rao, T. N.; Tryk, D. A.; Rao, T. N.; Tryk, D. A., *J. Photochem. and Photobio. :A* **2004,** *168*, 47–52.
44. S. K. Poznyak, D. V. T., A. I. Kulak, *J. Phys. Chem. B* **2002,** *105*, 4816–4823.
45. Y. Wu, L. H., Z. Jiang, Q. Ke, *J. Electrochem. Soc.* **1997,** *144*, 1728–1733.
46. P.Mallick, S. S., *Nanoscience and Nanotechnology* **2012,** *2(3)*, 71-74.
47. Mahdi Shahmiri, N. A. Z. I., Norhazlin Zainuddin, Nilofarasim, B Bakhtyar, A, *E-ISSN* **2013,** *9(3)*, 2224-3496.